ECS Journal of Solid State
Science and Technology

Synergistic Effect of Pad "Macroporous-Reactors" on Passivation Mechanisms to Modulate Cu Chemical Mechanical Planarization (CMP) Performance

ECS Journal of Solid State Science and Technology, 2020 **9** 054005

Synergistic Effect of Pad "Macroporous-Reactors" on Passivation Mechanisms to Modulate Cu Chemical Mechanical Planarization (CMP) Performance

Katherine M. Wortman-Otto,* Carolyn F. Graverson,* Abigail N. Linhart,* Rose K. McDonough, Amy L. Mlynarski, and Jason J. Keleher**,z**

Department of Chemistry, Lewis University, Romeoville, Illinois 60446-2200, United States of America

Decoupling the key interfacial mechanisms (chemical and mechanical) present during Cu CMP is critical to the development of slurry/pad consumable sets to reduce defectivity at advanced technology nodes. Understanding the Prestonian relationship, or lack thereof, can give rise to correlations between film density as a result of passivation film kinetics and thermodynamics as they relate to Cu oxidation/electrochemistry under dynamic conditions. The efficiency of film removability is strongly correlated to the molecular structure of the passivating agent and its synergistic relationship with the macroporous-reactor sites presented in this work. Results indicate that passivation film activation energy (E_a) is altered by the transport of fresh and waste slurry chemistry to the Cu interface via pad asperity contact. Furthermore, this work employs inhibitors with varying structural attributes to probe how the density of film formation is impacted by the efficiency of complexation and non-covalent interactions at the Cu surface. When comparing the best-in-class benzotriazole (BTA) with salicylhydroxamic acid (SHA), the triazole film formation is driven by a traditional complexation/π-stacking mechanism, while the hydroxamic acid film is the result of a colloidal supramolecular complex and soft surface-adsorption requiring reduced downforce for Cu removal.

 [DOI: 10.1149/2162-8777/ab9b05]

Manuscript submitted April 27, 2020; revised manuscript received June 2, 2020. Published June 16, 2020.

Chemical Mechanical Planarization (CMP) is a critical process step in extending Moore's Law and must be understood at a deeper, mechanistic level to limit defects that are detrimental to shrinking feature size.[1] This requires not only bulk Cu removal but also improved surface topography and global planarity, critical for building 3D NAND devices, which requires the removal of significant Cu overburden due to the implementation of through-silicon vias (TSV).[2–4] Current device architectures consist of Cu/low-κ layers as this combination results in the lowest current leakage as it resists electron migration between features, but still has low resistivity within the infrastructure of the integrated circuit.[4] In order to effectively planarize to achieve desired topography, Cu CMP employs a delicate balance between chemical action (slurry) and mechanical force (downforce) as a means of removing bulk Cu at the surface while modulating surface topography in the post-polish state. Variations in defects and surface topography may be a result of galvanic corrosion/pitting, micro-scratching, particle contamination, line dishing, or edge-over-erosion, among others.[5–10] Modulating the chemical and physical stress at the Cu/slurry/pad interface will be key to limiting post-CMP defects and is controlled by selectively altering slurry chemistry. A typical Cu CMP slurry is a colloidal dispersion of nanoparticles coupled with chemical components including: complexing agents, corrosion inhibitors (passivating agents), oxidizers, rheological modifiers (i.e. surfactants), and pH adjusters.[4,11–16] When Cu is removed from the bulk via equal parts chemical and mechanical action, this is known as a Prestonian relationship and is achieved when true abrasion is occurring.[17,18] However, when the chemical force dominates, corrosion is the main mechanism of removal and, as previously mentioned, can lead to defects in the surface topography. Therefore, the type of inhibitor used greatly changes the nature of Cu removal (i.e. corrosive/abrasive).[2,6,19–24] While there is large agreement within the community that benzotriazole (BTA) is a first-rate inhibitor, only a small sub-set of work has been done to probe its mechanism of complexation and how structural changes to the inhibitor alter its ability to limit corrosion.[14,25,26] Furthermore, the type of pad used (i.e. hard/soft) and pad composition/properties largely impacts the CMP performance, which has been attributed to the pad asperity contact and the different slurry transport profiles as many studies have investigated the effects of pad conditioning/surface roughness, flow rate, and the coefficient of friction.[9,10,27–33] While there has been some indication that the pad type correlates to the chemical interactions at the Cu/slurry/pad interface, it is necessary to further examine and validate the effects of chemical entrapment within pad asperities as they relate to corrosion inhibition modes. Better understanding the mechanism of Cu surface passivation from a dual perspective (i.e. chemical and physical) reveals the importance of inhibitor complexation mechanisms under dynamic conditions, which can be directly correlated to widely reported CMP performance metrics. This paper will attempt to unravel the complex synergy at the Cu/slurry/pad interface through a series of electrochemical measurements that reveal the dynamic activation energy (E_a) of film formation occurring during CMP.[34] Correlation of these E_a's to CMP trends in relationship to downforce and time will be discussed to solidify the role of pad macroporous-reactors in the development of structurally diverse inhibitor sets.

Experimental

Slurry formulation.—The Cu slurry formulation for this study was a silica-based slurry composed of 0.5 wt% of 60 nm colloidal silica (PL-3 obtained from Fuso Chemical Co.), 1 wt% glycine (99%, Sigma-Aldrich), 1 wt% H_2O_2 (30 wt%, JT Baker), and 100ppm of film formers. The 4 film formers studied for this publication were BTA (99.5%, Sigma-Aldrich), benzimidazole (BIA) (98%, Aldrich), 1,2,3-Triazole (TAZ) (98%, Aldrich), and Salicylhydroxamic acid (SHA) (99%, Acros Organics). An overall pH of 5.8 was achieved for all slurries formulated using KOH and HNO_3 as pH adjusters.

Material removal rate (MRR).—The downforce curves for this study were generated using an Allied MetPrep 4 grinder/polisher and a 3 mm copper disk (i.e. "slug") with a cross sectional area of 7.5 cm^2. The authors would like to recognize that there are differences between Cu disk samples and Cu wafer samples, however this study is looking at relative differences to better understand the removal mechanism. The polishing parameters were downforces of 0, 0.5, 1, and 2 psi, a platen speed of 100 rpm, and a slurry flow rate of 150 ml min^{-1}. It must be noted

*Electrochemical Society Student Member.
**Electrochemical Society Member.
zE-mail: keleheja@lewisu.edu

that before the slurry was pumped onto the polishing pad, it was evenly stirred with a magnetic stir bar in order to prevent the formation of large slurry aggregates. Polishing experiments were performed using both an IC-1000 pad (hard pad) and a Fujibo pad (soft pad), with 10 min of conditioning prior to each trial. The IC-1000 pad was conditioned with a diamond conditioner while the Fujibo pad was conditioned with a soft-bristled brush. In order to determine the MRR, the weight of the Cu slug was massed pre- and post-polish using a 5-point scale by Mettler-Toledo.

Hydroxyl radical (*OH) trapping.—The concentration of *OH generated was determined using a widely accepted methodology,[35] which uses UV–vis spectroscopy and p-nitrosodimethylanline (PNDA) as a probe molecule. The peak intensity of PNDA (97%, Sigma-Aldrich) occurs at 440 nm and when the PNDA reacts with *OH generated in the system, the peak intensity decreases. The *OH were generated according to a modification of a previously reported methodology, where a 1in. × 1in. Cu coupon was exposed to the slurry of interested (as prepared above) for the desired time frame. Samples were removed and the PNDA probe molecule was injected and mixed for 2 min prior to spectroscopic measurements using a Persee T7S UV–vis spectrophotometer.

Atomic force microscopy (AFM).—Atomic force microscopy (AFM) was utilized to assess pad surface structure/texturing at optimal Cu process conditioning time (i.e. 30 min). All scans were performed using the Nanosurf Flex AFM (Nanoscience Instruments) in contact mode with a Si probe from AppNano (SHOCON model). Each scan was 25 μm × 25 μm in size and measured with a scan rate of 1 s/line and 300 points/line.

Electrochemical analysis and E_a determination.—Potentiodynamic analysis (Tafel Analysis) was performed using a Gamry Reference 600 potentiostat. This set-up utilized a 3-electrode system which included a saturated calomel reference electrode, a platinum counter electrode, and a copper rotating disk working electrode at 25 °C and 45 °C. The sample area of the Cu electrode was determined to be 1.327 cm^2 with a density of 8.96 g cm^{-3}. The corrosion current (I_{corr}) values were obtained by measuring the current at the intersection of the tangent lines of the cathodic and anodic curves. These values were then normalized using the calculated sample area mentioned above. Once the I_{corr} was determined, the E_a was calculated using an extension of the Arrhenius relationship as shown below:

$$\ln(I_{corr}) = -\frac{E_a}{R}\frac{1}{T} + \ln(A)$$

Where A represents the Arrhenius constant, R represents the gas constant (8.3145 J·mol^{-1}·K^{-1}), and T is representative of the absolute temperature in Kelvin.

Results and Discussion

In order to effectively understand the synergy between Cu slurry formulations and CMP pad properties, it is imperative to study the polishing performance. More specifically, the relationship between inhibitor structure and pad asperity contact/polymer hardness was investigated at a macroporous level. Figure 1 shows the MRR of four slurries containing structurally diverse inhibitors, widely reported in Cu CMP literature, using an IC-1000 polyurethane pad.

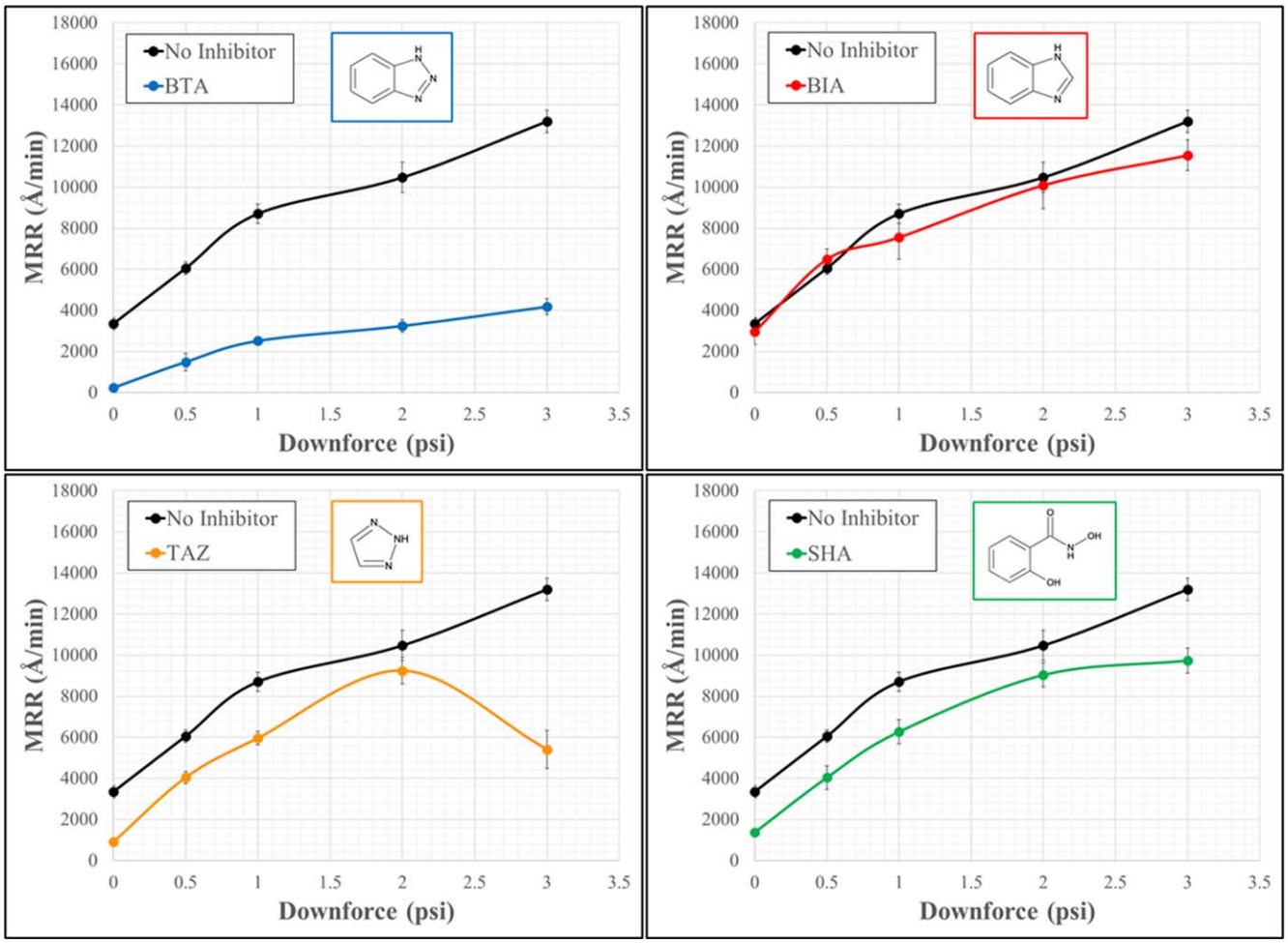

Figure 1. MRR as a function of downforce on an IC-1000 pad.

It must be noted that Prestonian CMP follows a linear relationship between MRR and downforce, where little to no Cu removal is seen at the 0 psi condition, showing characteristics of chemical activity (i.e. dynamic etch). Any deviation from this relationship is indicative of a chemical/mechanical imbalance. Results of the no inhibitor case clearly show a chemically active system because of the high MRR present at 0 psi. This etching can be attributed to the initial dissolution of the Cu^0 from the H_2O_2 present to Cu^{2+}. This ion is then easily complexed in solution by glycine, which in turn produces a higher concentration of *OH through Fenton decomposition. Furthermore, the no inhibitor shows two regimes of removal as the downforce is increased. The low downforce regime shows a linear relationship, indicative of a Prestonian-like removal process. At the higher downforce regime, however, the chemical activity dominates the removal mechanism as the rate no longer increases with downforce. This inflection point between the two regimes is indicative of a change in the slurry microenvironment where the temperature and mass transport of the chemistry affect the kinetic/thermodynamic equilibrium of film formation. BTA, as the most widely reported inhibitor in both publications and patents, stands as the foundational basis for most Cu CMP slurry formulations. At the 0 psi condition, there is minimal dynamic etch which falls in line with the Prestonian concept of CMP—a significant difference when compared to the no inhibitor case. It can be noted that at low downforce (0–1 psi), it loosely follows a Prestonian relationship but at significantly reduced rate, clearly indicating a shift to a mechanically dominant removal mechanism. This strong inhibition can be attributed to the formation of a dense passivation film resulting from the interfacial complexation of Cu^+ coupled with effective π-stacking from the aromatic moiety present in BTA. Again, however, there is an inflection point ($\sim$1 psi) where the chemical activity of film formation reaches a critical point in which the kinetic/thermodynamic microenvironment is optimal. Changing the structural backbone from a macrocyclic triazole (BTA) to a macrocyclic imidazole (BIA) results in significant degradation of passivation efficiency as demonstrated by its similar MRR to the no inhibitor case. This can be directly attributed to the inability to intercept Cu^+ resulting in weak chemisorption and relying only on π-stacking as the main mode of film formation. On the other hand, removing the aromatic ring from BTA (i.e. resultant TAZ molecule) reveals the critical role of π-stacking in passivation dynamics. Again, referring back to the 0 psi condition, there is a slight increase (677 Å min^{-1}) in dynamic etching yet still exhibiting significant Prestonian behavior at a longer downforce range (0–2 psi). While TAZ has similar ability to promote interfacial Cu^+ complexes as BTA, it has a significantly higher MRR due to the lack of π-stacking in the system (i.e. weaker passivation film). However, at higher downforce (3 psi) there is increased physical transport of slurry and waste components providing greater local concentration of inhibitor complexes at the Cu surface. This increase in local concentration, in conjunction with the kinetic/thermodynamic conditions, results in enhanced passivation evident in the significant decrease in MRR. This phenomenon can be described as "physically induced chemical passivation." In contrast to the other inhibitors, SHA is not widely studied as a passivating agent in Cu CMP. At the 0 psi condition, it is similar to TAZ in that dynamic etch is present at mitigated levels, but the mode of inhibition is more likely a Cu^{2+}-SHA complex, therefore behaving more like glycine. This is further supported by the Prestonian-like behavior over a long downforce range (0–2 psi) and the evident increase in chemical activity at higher downforce (3 psi).

In order to test the robustness of the inhibitor film, modulation of the mechanical environment was explored using a soft, Fujibo pad. It has been reported that soft pads are more porous and have greater pad/asperity contact than traditional hard pads (i.e. IC-1000). While the complexation mechanism of film formation is not significantly altered, the mechanical delivery of the inhibitor to the Cu surface will be impacted by pad type used. Figure 2 is a summary of MRRs for each inhibitor type on a Fujibo pad. In comparison to the IC-1000 case, the no inhibitor slurry shows the same dynamic etch rate on the Fujibo pad signifying consistent chemical activity. The CMP polish rates are higher and more Prestonian-like across the entirety of the downforce curve, indicating a difference in the amount of slurry at the pad/wafer interface. On the other hand, BTA shows no significant change in either absolute rate or profile. This result indicates that the nature of the BTA film formation is not dependent on pad/wafer contact because of the dense passivation layer formed. In the case of BIA, there is a similar response as the IC-1000 pad where the passivation is limited via the aforementioned film formation mechanism. As a result of BIA's poor performance as an inhibitor, its complexation and delivery mechanism will not be explored further as it is not a viable option for contributing to this mechanistic study. A significant differentiating point occurs upon examination of the TAZ and SHA MRR profiles. While the complexation mechanisms remain consistent, TAZ shows a shift in the peak MRR to a lower downforce regime. As downforce increases, the slurry retained in the macroporous pad asperities is released more effectively upon pad compression altering the kinetics/thermodynamics of film formation. Similarly, the MRR profile for SHA shows a similar shift to greater passivation at a lower downforce regime as compared to IC-1000. Based on this, it is hypothesized that the macropore environment is serving as a potential slurry reservoir (i.e. in situ macroporous-reactor).

Figure 3 is an AFM topographical representation as a function of pad type which illustrates potential sites for the evolution of in situ macroporous-reactors. Comparing a representative sample set (n = 10) of IC-1000 and Fujibo pads, there is a significant difference in the peak to valley distribution at optimal pad conditioning. This increase in surface roughness in the soft pad clearly shows the presence of pad asperities and the macropores that exist between them, which can act as reservoirs for slurry retention. These reservoirs can significantly modulate the film formation dynamics of TAZ and SHA resulting in the previously shown polishing profile shifts.

In order to fully understand and exploit the aforementioned chemical-mechanical interactions it is necessary to utilize molecular-scale analytical techniques to interrogate the Cu surface. Literature describes the Cu CMP process as a complex set of redox reactions and coordination chemistry that drive the kinetics and thermodynamics of removal and passivation, all in harmony with the mechanical forces. One such way to analyze this is through potentiodynamic analysis (i.e. Tafel plots) to monitor the oxidation of Cu^0 to Cu^+ to Cu^{2+} and its dissolution from the bulk surface.[36–38] More specifically, the ability of the inhibitors described in this work to modulate this removal in a constructive fashion (i.e. non-dissolutive nature). Traditionally this work is performed in a highly controlled environment to minimize external factors (substrate properties, oxygenated environment, no mixing profile, etc.) that could alter the nature of the passivation film formation kinetics and thermodynamics. However, this work employs an electrochemical technique that looks at "real-time" potentiodynamic scans using model slurry systems and conditioned pads (hard/soft) to simulate abrasive CMP conditions. Figure 4 is a summary of potentiodynamic scan analysis for both pads at a moderate downforce of 1.5 psi.

In the IC-1000 case, the open circuit potential (OCP) shows the expected trend, as BTA (230 mV) is the most passive in nature and no inhibitor (80 mV) shows the greatest corrosive behavior as the only inhibition film present is H_2O_2 overoxidation to CuO. This finding supports the previous claims that BTA had the greatest suppression of MRR at all downforce conditions. Additionally, the soft pad Tafel analysis supports the previous claim that the BTA slurry (202 mV) induces the most passivation as it shows a large shift from the corrosive, no inhibitor slurry (106 mV). This again supports the claim that BTA is a rate suppressant for all downforces when compared to the no inhibitor condition. These findings give credence to the dense protective layer that requires significant mechanical force to remove upon formation. By making subtle structural changes, such as in TAZ and SHA, there are also critical shifts in the OCP compared to that of the best-in-class inhibitor,

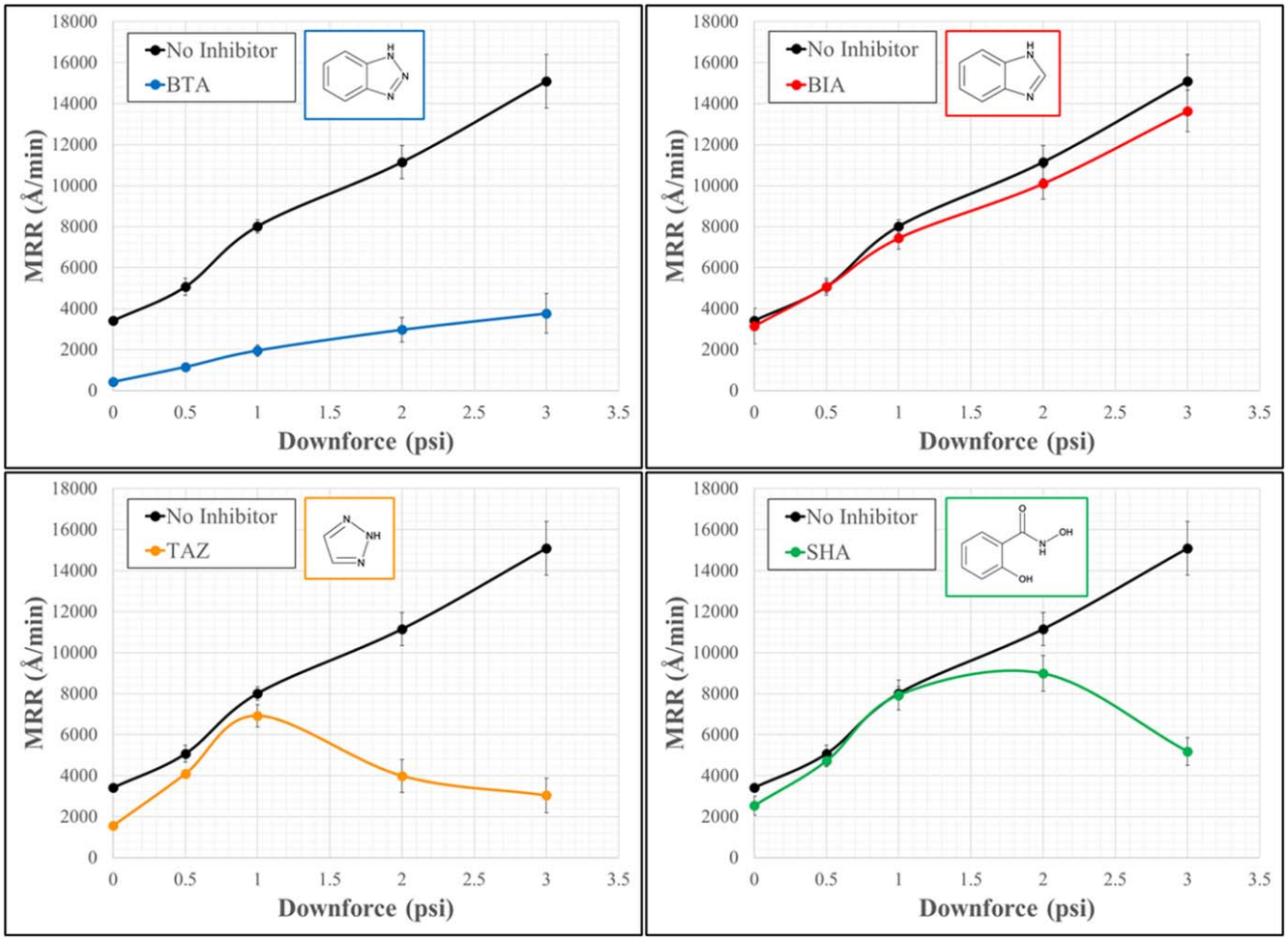

Figure 2. MRR as a function on a Fujibo pad.

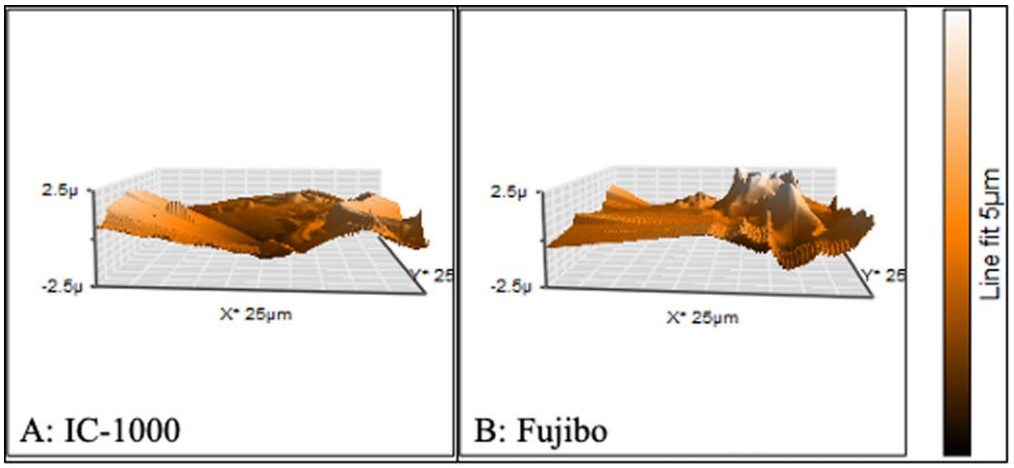

Figure 3. Representative AFM topographical images of in situ macroporous-reactors.

BTA. It must be noted that "best-in-class" inhibitor not only refers to effective passivation performance, but also the downforce curve linearity which allows for the desired process engineering flexibility required in planarization. On the IC-1000 pad, both TAZ and SHA show an increase in passivation when compared to the no inhibitor case. This indicates a shift in the mechanism of film formation that can be directly tied to the inhibitor structure. More specifically, while TAZ (120 mV) has the same surface coordinating nature as BTA, the removal of the aromatic ring limits its π-stacking efficacy thus changing the effective packing strength at the Cu surface. This reduction of surface rigidity will substantially reduce its passivation efficiency under dynamic conditions as shown in the MRR curves. On the other hand, SHA (163 mV) shows significantly improved corrosion control approaching BTA-like passivation efficiency. However, the mechanism of passivation differs greatly as the aromatic hydroxamic acid functionality provides π-stacking capacity, but the Cu complexes (Cu^{+} vs Cu^{2+}) are different. Although the passivation is similar, the MRR curves vary greatly thus giving

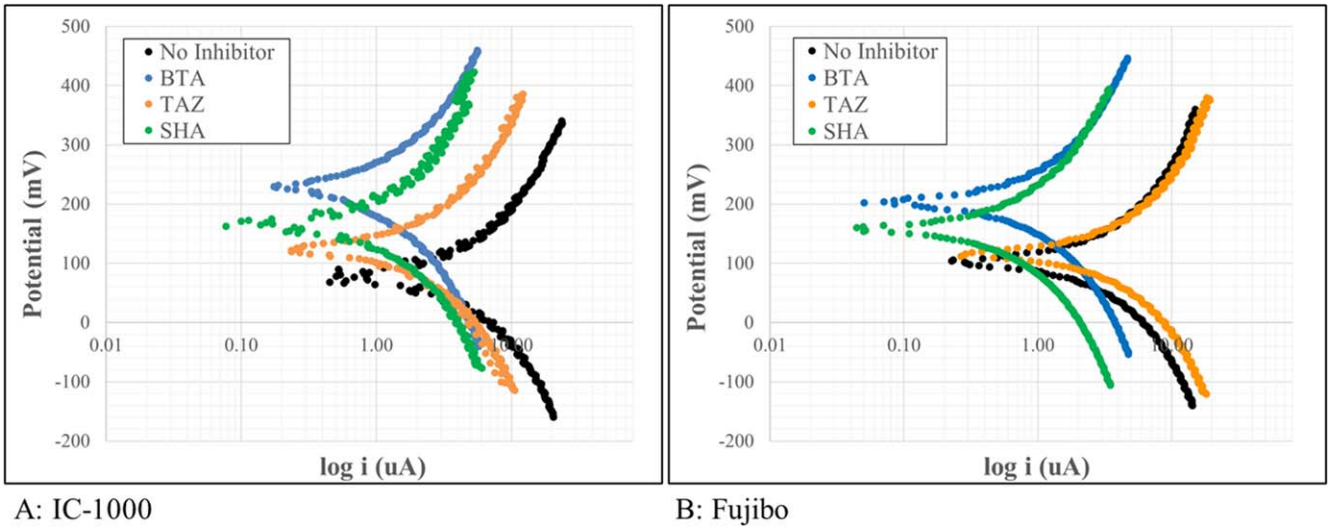

Figure 4. Dynamic Tafel analysis of each inhibitor on IC-1000 and Fujibo.

insight into the differences in film density. This is even further supported by the Tafel analysis on the Fujibo pad which shows limited change in SHA's passivation characteristics, but significant change for the TAZ slurry. For TAZ (112 mV), the passivation is very similar to the no inhibitor condition which indicates as the asperity contact increases, the weakly surface-adsorbing TAZ is rendered ineffective. For SHA (160 mV), on the other hand, the OCP does not change, therefore indicating the mode of film formation is not directly related to surface complexation, rather it is more dependent on the transport of active chemistry to the surface.

While OCP can describe the macroscopic nature of the passivation film, it is necessary to understand the dynamic processes at the interface. Furthermore, the Tafel relationships can give the corrosion rate for the various inhibitors under the chosen conditions previously described. By employing a simple Arrhenius relationship, the E_a changes for the Cu oxidation reaction can be determined for each inhibitor/pad combination under CMP conditions, and is summarized in Table I.

An overarching theme is that the inhibitor E_a follows the expected trend (BTA > SHA > TAZ > no inhibitor) based on both polish rate and OCP measurements. However, a deeper dive into the relative differences between each inhibitor at 2 different downforces for both pads reveals significant information about the kinetics and thermodynamics of film formation. At the 0 psi condition, which represents the dynamic etch (where the Cu is rotating while in contact with the pad, but there is no applied load) there are stark differences between IC-1000 and Fujibo. For all inhibitors, there was a drop in the E_a when moving from IC-1000 to Fujibo, which can be directly related back to the relationship between asperity contact and film density. Referring to the MRRs at 0 psi, there is a different trend where no inhibitor (3349 Å min^{-1}) is greater than TAZ (908 Å min^{-1}) and significantly greater than BTA (231 Å min^{-1}) but is about equal to SHA (1373 Å min^{-1}). Both BTA and TAZ behave as expected at both downforce conditions due to their previously described surface passivation mechanisms. On the other hand, SHA exhibits a unique passivation mechanism giving rise to non-traditional rate control. While traditional inhibitors, like BTA, complex with the surface Cu^+, SHA has a higher affinity for Cu^{2+}.

It has been widely reported that the Cu^{2+}-glycine complexes formed during the CMP process catalytically decompose H_2O_2 to *OH. By monitoring the radical generation using a trapping technique, one can validate the effect of inhibitor on the in situ generation of *OH. Figure 5 is a summary of *OH generation as a function of time in the presence of BTA and SHA. The BTA film density is a result of its ability to complex with Cu^+ and π-stack at the Cu surface, preventing it from oxidizing further to Cu^{2+}. On the other hand, SHA complexes with Cu^{2+} that has oxidized into solution and must compete with the glycine in the system. It is believed that the SHA-Cu complexes do not allow for Fenton

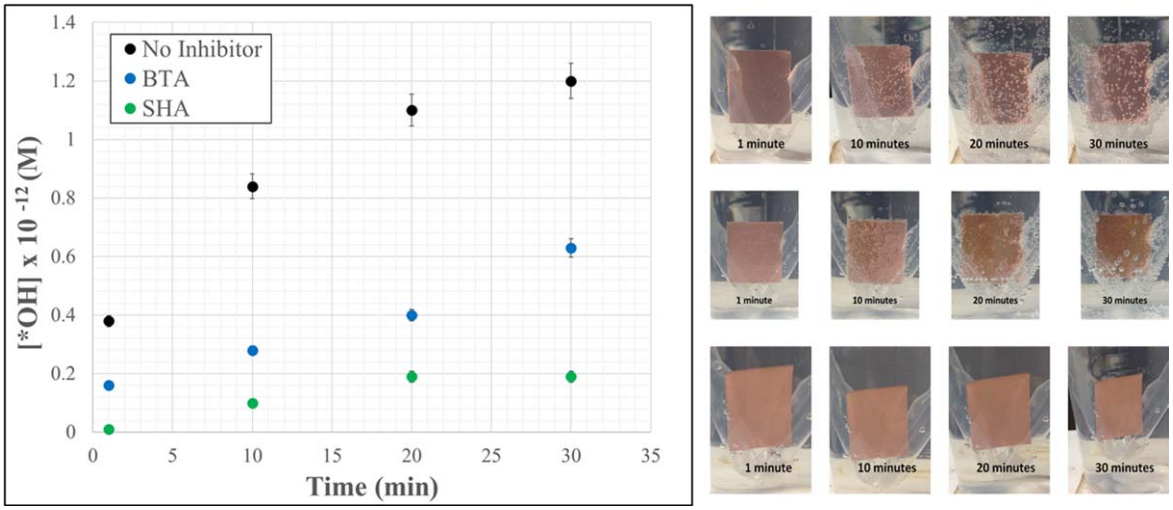

Figure 5. *OH trapping under dynamic etch conditions in the presence of BTA and SHA.

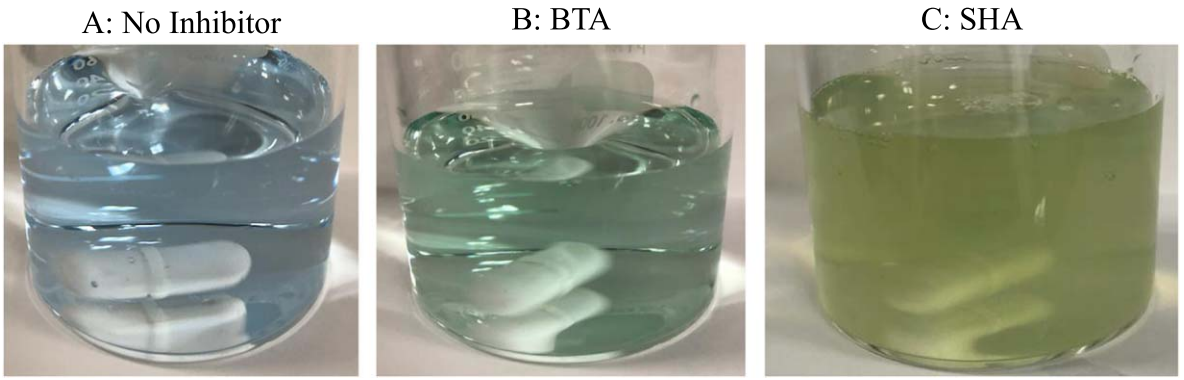

Figure 6. Visual comparison of soluble and insoluble complexes in the presence of BTA and SHA.

decomposition to occur and instead can non-covalently interact with free glycine in solution to become soft, colloidal supramolecular structures. Upon efficient transport, these supramolecular structures may passivate the Cu surface in a mechanism designated as "physically induced chemical passivation." Clear evidence for this claim, as seen in Fig. 6, is the change in opacity of the post-static etch waste for SHA compared to that of soluble Cu^{+}-BTA and Cu^{2+}-glycine complexes. In addition, looking at the high downforce MRRs shows a suppression in the SHA slurry MRR on the Fujibo pad which can be directly related to an increase in E_a under downforce applied electrochemical analysis. It is believed that upon increased local pressure on the Fujibo pad, the asperities are compressed to release the colloidal supramolecular structures to the Cu surface, which in turn suppresses the overall MRR. This finding clearly demonstrates that the transport of chemistry (fresh or waste) is critical in controlling the kinetics and thermodynamics of passivation. Furthermore, as previously mentioned, the macro-porous-reactors present on the Fujibo pad (i.e. asperity and void volume) synergistically enhance these passivation mechanisms.

To further support this claim, the 0 psi MRR of select inhibitors were investigated as a function of polish time. This condition was selected to provide an accurate depiction that the role of Cu ion formation ($Cu^0 \rightarrow Cu^+ \rightarrow Cu^{2+}$) plays in the inhibition film formation and how even minimal asperity contact impacts its subsequent removal. Figures 7 and 8 are a summary of dynamic removal under limited downforce on both IC-1000 and Fujibo pads.

In the case of IC-1000, there is a clear initial MRR for all cases that is a result of Cu^0 oxidizing but the magnitude of this increase is

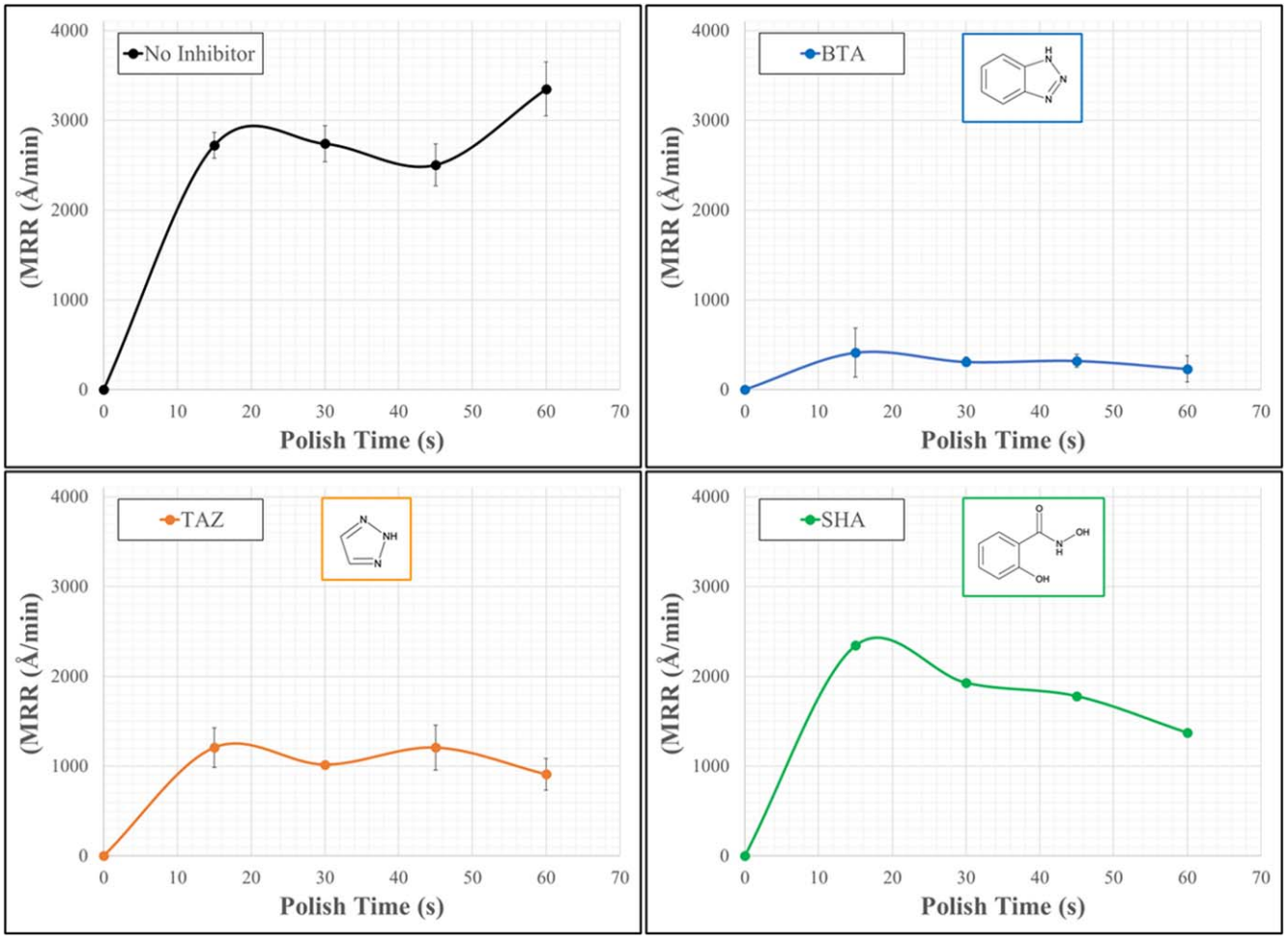

Figure 7. MRR as a function of time at the 0 psi condition on IC-1000.

Table I. Inhibitor E_a's on IC-1000 and Fujibo.

	IC-1000 Pad		Fujibo Pad	
	E_a (kJ mol^{-1})		E_a (kJ mol^{-1})	
Inhibitor	0 psi	2 psi	0 psi	2 psi
None	0.8 ± 0.1	16.6 ± 2.1	0.0 ± 0.0	8.4 ± 1.0
BTA	84.6 ± 10.6	100.4 ± 12.6	60.4 ± 7.6	97.4 ± 12.2
TAZ	16.9 ± 2.0	43.2 ± 5.2	2.6 ± 0.3	41.2 ± 5.1
SHA	62.5 ± 7.5	33.7 ± 4.2	45.7 ± 5.5	78.7 ± 9.8

driven by the mechanism of passivation. The no inhibitor slurry shows the highest MRR for all times as the only inhibition mechanism is the formation of CuO which is kinetically slower than the static etch from *OH. Inhibitors with triazole functionality exhibit reduced rate with minimal time dependent variation, indicating a strong surface adsorbing interaction as described previously. When comparing BTA and TAZ, however, BTA shows greater MRR suppression thus indicating the importance of π-stacking for surface adsorption and subsequent film density. On the other hand, SHA demonstrates glycine dominant complexation in a short time range (i.e. 0–15 s) due to the large, local concentration gradient present. Over time, though, the hydroxamic acid functionality complexes with Cu^{2+} and non-covalently interacts with glycine to form colloidal supramolecular structures, trapped in pad macroporous-reactors, and subsequently transported to the Cu surface resulting in delayed passivation.

In comparison, Fujibo pad yields higher MRRs for all times and inhibitor structures. This observation further validates pad-asperity macroporous-reactor content is significantly different between IC-1000 and Fujibo pads. For the no inhibitor system, there is a significant change in the MRR which continually increases as a function of time, indicating that the local concentration of reactive chemistry is creating enhanced Cu dissolution, which is known to increase post-CMP defects (i.e. corrosion and non-uniform topography). While the passivation trends hold true (BTA > TAZ/SHA) and are supported by previously mentioned electrochemical results, there is a unique oscillatory shape in MRR as a function of time. It is believed that this is related to increased asperity contact and void space which is related to the kinetic and thermodynamic formation of the film. It must be noted that in the no inhibitor case, there is a slight oscillatory profile which can be attributed to attaining the necessary concertation of Cu^{2+}-Glycine complexes in order to catalytically generate a sufficient amount of *OH to achieve a chemically activated MRR. More specifically, in the case of both TAZ and SHA, there is an initial oxidation phase at the short time frame in which the Cu substrate undergoes glycine-like removal mechanisms. At increased polish times (30–45 s), the substrate experiences local concentration changes in the macropore validating the effective delivery of inhibitor chemistry resulting in clear rate suppression. Furthermore, at 60 s, there is a drastic increase in MRR for both inhibitors, shifting the equilibrium of the concentration gradient back toward a glycine dominant mechanism, through a non-pressure induced dynamic delivery of the slurry. As previously shown, upon the addition of pressure at the 60 s time (Figs. 2 and 3), in both the TAZ and SHA case, there is a reduction in overall MRR

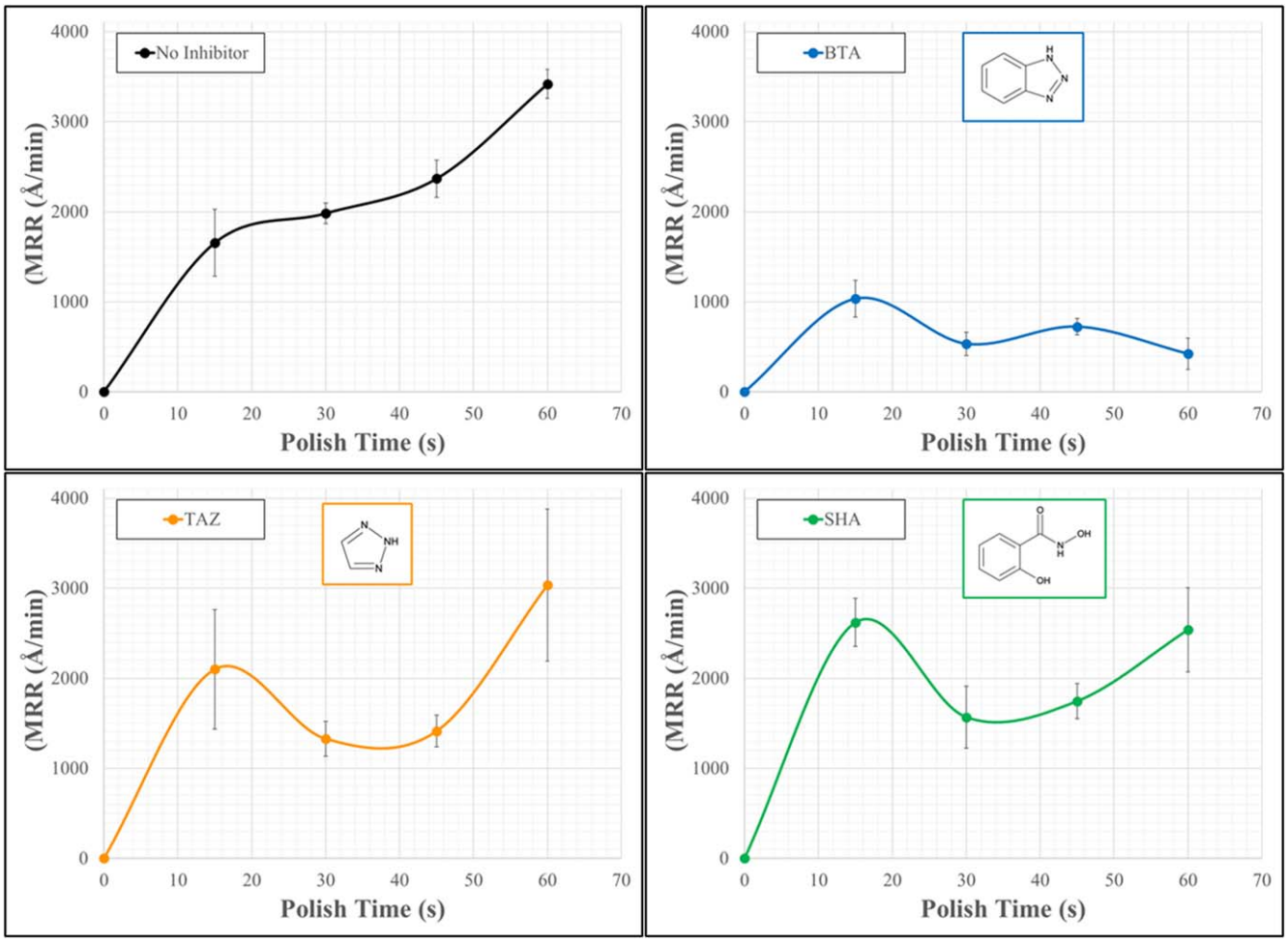

Figure 8. MRR as a function of time at the 0 psi condition on Fujibo.

under the Fujibo pad signifying the role of the macroporous-reactor in high pressure, and pressure reduced conditions.

Conclusions

This work generates results to further support that pad/slurry synergy is beyond a mechanical interplay and instead contributes to the transport of chemistry resulting in modulating the kinetics and thermodynamics of critical film formation at the Cu interface. Results clearly indicate the role of macroporous-reactor sites on the E_a of passivation film formation is critical to the mode of Cu removal (i.e. chemical/mechanical). It must be noted that BTA remains as the best-in-class inhibitor primarily because of its ability to complex (via triazole functionality) as a dense film that requires significant mechanical abrasion to remove and may result in surface micro-scratches. Additionally, by simply disrupting the triazole functionality (i.e. BIA) there was poor passivation efficacy, rendering it ineffective as a passivating agent in Cu CMP. The secondary mode of dense film formation is because of BTA's strong surface adsorption through π-stacking, which was validated by removing the aromatic ring in TAZ and seeing an increase in MRR and reduction in E_a. Conversely, SHA inhibits in a unique fashion such that it competes with glycine to complex with Cu (validated by reduction in generated *OH), resulting in colloidal supramolecular complexes that require effective delivery to the substrate surface. This results in a soft passivation film that relies on control of the corrosion environment to limit defects. Results validate that inhibitors should be selected dependent on their mechanism of passivation to fully understand potential resulting defect types.

Acknowledgments

The authors would like to thank Allie Mikos, Maria G. Salinas, and Cynthia Saucedo for their value-added contributions.

ORCID

Katherine M. Wortman-Otto https://orcid.org/0000-0003-4905-140X
Carolyn F. Graverson https://orcid.org/0000-0001-5739-0757
Abigail N. Linhart https://orcid.org/0000-0002-6540-8248
Jason J. Keleher https://orcid.org/0000-0003-4310-6094

References

1. J. Shalf, *Philos. Trans. R. Soc. A Math. Phys. Eng. Sci.*, **378**, 1 (2020).
2. P. C. Lin, J. H. Xu, H. L. Lu, D. W. Zhang, and P. Li, *J. Semicond. Technol. Sci.*, **17**, 319 (2017).
3. S. Tominaga, D. Abe, T. Enomoto, S. Kondo, H. Kitada, and T. Ohba, *Jpn. J. Appl. Phys.*, **49**, 1 (2010).
4. B. Hu, H. Kim, R. Wen, and D. Mahulikar, *ECS Trans.* (ECS) Vol. 18, p. 479 (2009).
5. T. B. Zubi, R. A. Wiencek, A. L. Mlynarski, J. M. Truffa, K. M. Wortman-Otto, C. Saucedo, M. G. Salinas, C. F. Graverson, and J. J. Keleher, *ECS J. Solid State Sci. Technol.*, **8**, P3022 (2019).
6. C. H. Chao, J. F. Wang, Q. Ye, S. H. Wu, B. Chi, S. Y. Chen, W. C. Yu, and P. C. Liu, in*ECS Trans.* (The Electrochemical Society) Vol. 44, p. 525 (2012).
7. Y. Hong, V. K. Devarapalli, D. Roy, and S. V. Babu, *J. Electrochem. Soc.*, **154**, H444 (2007).
8. J. Yu, D. Jia, S. S. Venkataraman, and Y. Li, *J. Electrochem. Soc.*, **157**, H312 (2010).
9. S. Kim, N. Saka, and J.-H. Chun, *ECS J. Solid State Sci. Technol.*, **3**, P169 (2014).
10. D. C. Ponte and D. M. L. Meyer, *J. Mater. Sci., Mater. Electron.*, **27**, 1745 (2016).
11. C. Liao, D. Guo, S. Wen, and J. Luo, *Tribol. Lett.*, **45**, 309 (2012).
12. Y. Ein-Eli, E. Abelev, E. Rabkin, and D. Starosvetsky, *J. Electrochem. Soc.*, **150**, C646 (2003).
13. T. H. Tsai and Y. F. Wu, *Chem. Eng. Commun.*, **193**, 702 (2006).
14. B. J. Cho, S. Shima, S. Hamada, and J. G. Park, *Appl. Surf. Sci.*, **384**, 505 (2016).
15. M. Nagar, D. Starosvetsky, J. Vaes, and Y. Ein-Eli, *Electrochim. Acta*, **55**, 3560 (2010).
16. R. K. Singh and R. Bajaj, *MRS Bull.*, **27**, 743 (2002).
17. M. Ziomek-Moroz, A. Miller, J. Hawk, K. Cadien, and D. Y. Li, *Wear*, **255**, 869 (2003).
18. V. Rastegar and S. V. Babu, *China Semicond. Technol. Int. Conf. 2017, CSTIC 2017* (2017).
19. A. Goswami, S. Koskey, T. Mukherjee, and O. Chyan, *ECS J. Solid State Sci. Technol.*, **3**, P293 (2014).
20. G. Yang, H. Wang, N. Wang, R. Sun, and C. P. Wong, *J. Alloys Compd.*, **770**, 175 (2019).
21. W. Ning, P. Guoshun, and L. Yan, *Microelectron. Eng.*, **88**, 3372 (2011).
22. Y. Wang and Y. Zhao, *Appl. Surf. Sci.*, **254**, 1517 (2007).
23. W. Huang, S. Tamilmani, S. Raghavan, and R. Small, *Int. J. Miner. Process.*, **72**, 365 (2003).
24. Q. Wang, B. Tan, B. Gao, S. Tian, C. Han, and L. Yang, *ECS J. Solid State Sci. Technol.*, **8**, P313 (2019).
25. S. Deshpande, S. C. Kuiry, M. Klimov, and S. Seal, *Electrochem. Solid-State Lett.*, **8**, G98 (2005).
26. Y. H. Lei, N. Sheng, A. Hyono, M. Ueda, and T. Ohtsuka, *Prog. Org. Coatings*, **77**, 339 (2014).
27. J. Yi, *IEEE Trans. Semicond. Manuf.*, **18**, 359 (2005).
28. A. Prasad, G. Fotou, and S. Li, *J. Mater. Res.*, **28**, 2380 (2013).
29. Z. Li, P. Lefevre, I. Koshiyama, K. Ina, D. Boning, and A. Philipossian, *IEEE Trans. Semicond. Manuf.*, **18**, 681 (2005).
30. R. Han, Y. Mu, Y. Sampurno, Y. Zhuang, and A. Philipossian, *ECS J. Solid State Sci. Technol.*, **6**, P201 (2017).
31. Y. Zhuang, X. Liao, L. J. Borucki, S. Theng, X. Wei, T. Ashizawa, and A. Philipossian, *ECS*, p. 599 (2010).
32. S. Li, G. Gaudet, and J. Nair, *ECS J. Solid State Sci. Technol.*, **2** (2013).
33. A. J. Khanna et al., *ECS J. Solid State Sci. Technol.*, **8**, P3063 (2019).
34. M. L. White, L. Jones, and R. Romine, *MRS Proceedings*, **1249**, 1249-E04–07 (2010).
35. M. Hariharaputhiran, J. Zhang, S. Ramarajan, J. J. Keleher, Y. Li, and S. V. Babu, *J. Electrochem. Soc.*, **147**, 3820 (2000).
36. M. Finšgar and I. Milošev, *Corros. Sci.*, **52**, 2737 (2010).
37. A. Kokalj, *Faraday Discuss.*, **180**, 415 (2015).
38. J. B. Cotton and I. R. Scholes, *Brit. Corros. J.*, **2**, 1 (1967).